Int J Thermophys (2007) 28:2019–2027
DOI 10.1007/s10765-007-0290-z

The Dependence of the Melting Temperature of Cobalt–Carbon Eutectic on the Morphology of its Microstructure

D. Lowe · K. Mingard · Z. Malik · P. Quested

Published online: 8 November 2007

Abstract Fixed points provide a reliable way to realize and verify temperature scales. High-temperature fixed points are being developed based upon alloys, since single-phase materials are impractical to use above the copper freezing point. In particular, eutectic alloys have been shown to be sufficiently reproducible to warrant consideration as a way to significantly improve high-temperature metrology. However, eutectic alloys have certain characteristics requiring that they are used differently from the current ITS-90 fixed points. As their freezing temperature depends on the freezing rate, the melting temperature is preferred, though it has been shown that for some alloys, notably iron–carbon and cobalt–carbon, the apparent melting temperature can depend on the rate of the preceding freeze. This behavior will need to be explained and quantified if such fixed points are to be acceptable. The effect of varying the freezing rate on subsequent melting has been investigated for cobalt–carbon eutectic fixed points. The apparent melting temperature varies by up to 50 mK. Measurements were made of two different fixed-point blackbodies with very similar results. Optical microscopy of samples produced at different freeze rates shows a change in scale of the microstructure. Electron back-scatter diffraction (EBSD) shows evidence of high levels of residual strain in rapidly frozen samples. The effect of annealing on the melting behavior and microstructure has also been investigated. It is suggested that disordered phase boundaries and residual strain lead to changes in the melting behavior as nonequilibrium conditions may lead to a significant level of pre-melting. Whether this actually changes the liquidus temperature, or whether the melting temperature

D. Lowe (✉) · K. Mingard · P. Quested
Industry and Innovation Division, National Physical Laboratory, Hampton Road, Teddington, Middlesex, TW11 0LW, UK
e-mail: dave.lowe@npl.co.uk

Z. Malik
Imperial College, London, UK

variation is due to the way the melting point is defined, is also discussed. The variation requires consideration if the highest accuracy is to be achieved, and will be a contributory factor to any uncertainty budget.

Keywords Eutectic · Melting temperature · Microstructure

1 Introduction

The idea of measuring the thermodynamic temperature of phase changes of particular materials and then using these as reference values to build a practical temperature scale was first suggested in 1889 [1]. Such fixed points are still fundamental to the current incarnation of the International Temperature Scale, ITS-90. Today, considerable effort is being put into extending the useful range of such scale-defining fixed points from 1,084°C (freezing point of copper) to 2,500°C [2], and perhaps even above 3,000°C [3]. This involves the use of eutectic alloys of metal and carbon (or of metal-carbides and carbon).

ITS-90 generally specifies the freezing temperature as the reference value. In this case, the system starts from a known initial condition and this homogenous liquid state is often maintained for several hours before solidification commences. The liquid is assumed to have no microstructure and impurities are evenly dispersed. In contrast, melting starts with an inherent microstructure determined by its solidification and subsequent thermal history, and impurities may have been unevenly distributed during the preceding freeze. Unfortunately, in the case of eutectic alloys, the freezing temperature is known to depend on the solidification rate. The need for atoms to diffuse from the uniform liquid to the segregated solid phases affects the shape of the solid–liquid interface. Faster freezing imposes shorter diffusion distances and, thus, a finer eutectic structure with consequently greater interfacial curvature. The excess surface energy of the curved solid–liquid interface means it is at a lower temperature than would be the case for true equilibrium [4]. Whether this effect is enough to preclude the eutectic freezing temperature as a reference point is not yet established. However, it is certainly the case that most researchers have reported that melting curves are more repeatable than freezing curves [2]. For this reason, research has tended to concentrate on melting temperature repeatability and reproducibility between sources. As a matter of practicality, it is found that melting takes place over a temperature range, and so the point-of-inflexion (POI) in the melt curve is taken to define the melting temperature. It is this feature of the melting curve that is found to be very repeatable. Inspection of an equilibrium phase diagram for a eutectic alloy shows that the eutectic temperature should be invariant. This suggests that if melting takes place over a significantly greater temperature range than conventional fixed points of comparable purity, then the system is not at equilibrium. It was reported [5,6] that although the melting curve POI does not depend on the melting rate, it could in some cases depend on the rate at which the preceding freezing takes place. This suggests that the melting curve depends on the microstructure (or possibly on an uneven distribution of impurities). This effect was relatively large for Fe–C (as much as 200 mK) and was clearly correlated to the scale of the eutectic microstructure. The reported effect was smaller for cobalt–carbon

(a lowering by 40 mK was observed), and the effect was absent for palladium–carbon. This article presents results of the preceding freezing rate on the melting temperature and microstructure of cobalt–carbon eutectic alloy.

2 Experimental

Two cobalt–carbon cells were used. Cell 2 (nominally <10 ppm impurities, metals basis) had a wider melting range, indicating lower quality than Cell 1 (nominally <20 ppm impurities). Unfortunately, Cell 1 broke, so we only have limited data for this cell. The fixed points were placed in a Lenton 3-zone open ceramic tube-furnace. This had an argon purge from the front and back, with graphite scavenger blocks at front and back. The front block would erode (oxidize) but, apart from some early superficial damage to the fixed-point crucible, it was possible to leave the crucible at high temperature for several days. The furnace end-zone offsets were adjusted to give a region uniform to ±0.2 K along the length of the crucible at 1,598 K.

To carry out a melt or freeze, the set point of the furnace was ramped at $0.3\,\mathrm{K}\cdot\mathrm{min}^{-1}$ to its new value and then held constant. The furnace controller is able to hold the furnace to within 0.1 K over many hours. An IKE LP2 or LP3 radiation thermometer (both operating at a nominal 650 nm wavelength with a 20 nm FWHM and 1 mm target size) determined the radiance temperature. Freezing was done at different solidification rates by holding the furnace set point temperature at different values below the eutectic temperature (T_e), from $T_e - 1\,\mathrm{K}$ to $T_e - 30\,\mathrm{K}$. Annealing of samples frozen with a $T_e - 20\,\mathrm{K}$ set point was performed for varying times up to 54 h at $T_e - 20\,\mathrm{K}$.

All melts were carried out under standardized conditions, with the fixed point stabilized at $T_e - 10\,\mathrm{K}$, then the furnace increased to $T_e + 10\,\mathrm{K}$ at a rate of $0.3\,\mathrm{K\,min}^{-1}$. Since the melting was carried out under almost identical conditions and only temperature differences were investigated, most of the uncertainty components that would be involved in an absolute temperature measurement either cancel out (e.g., the size-of-source effect is assumed to be the same for all measurements) or can be ignored (e.g., the reference photocurrent for ITS-90 realization) The remaining uncertainties were assumed to consist solely of the repeatability of the fixed-point realization (which combines the fixed-point stability and short-term pyrometer stability) and the day-to-day stability of the pyrometer. To test the stability of the experimental arrangement, a set of five successive cobalt–carbon fixed-point melting curve measurements were made following freezing at $T_e - 20\,\mathrm{K}$. The day-to-day stability was assessed from the repeatability of the melting temperature difference between $T_e - 2\,\mathrm{K}$ and $T_e - 20\,\mathrm{K}$.

To prepare material to assess microstructural changes, graphite sample holders with eutectic alloy ingots approximately 6 mm in diameter by 10–12 mm in length were placed directly behind the crucible as freezing was carried out. The high furnace uniformity assured that the samples received almost identical (within 0.5 K) thermal conditions to the fixed point. After sectioning, the samples were polished using Struer's Prematic 2, and finished with a colloidal silica polish to leave minimal polishing damage. For optical examination, samples were etched with a mixture of HF:HNO_3:Ethanol 7.5:2.5:200.

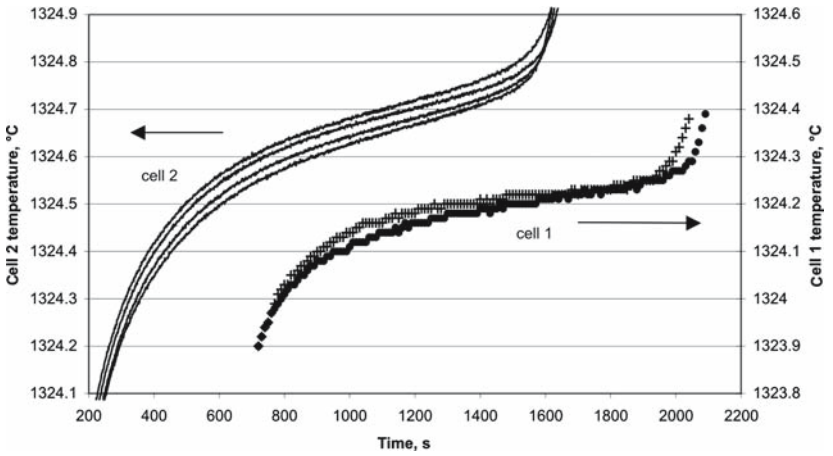

Fig. 1 *Left scale*: series of melts of Cell 2 following freezing at different rates; from top to bottom at $T_e - 1\,K$, $T_e - 2\,K$, $T_e - 10\,K$, and $T_e - 30\,K$ measured with the LP3. *Right scale*: two melts of cell 1 following freezing at $T_e - 2\,K$ (+) and $T_e - 20\,K$ (•)

The samples were examined optically to assess the differences in scale resulting from varying the freezing rate or annealing time. In addition, a fast-frozen sample and a slow-frozen sample were mapped using electron beam backscatter diffraction (EBSD). This electron microscopy technique maps the crystallographic orientation of a chosen cross-sectional area, and so can determine the grain structure within the cobalt-rich eutectic matrix. By measuring the misalignment between each point mapped (pixel) and its neighbors, a map quantifying the local residual strain imposed by solidification can be obtained.

3 Results

A typical melting curve series is shown in Fig. 1 for Cell 2. Cell 1 had limited data, some of which are also shown. The size of the temperature depression effect is similar for both the cells measured; the difference between $T_e - 1\,K$ and $T_e - 30\,K$ was 50 mK for both Cell 1 and Cell 2. Cell 1 appears to show a difference in melting curve quality, with the slower frozen one being flatter. With Cell 2, the more rapidly frozen sample consistently melted at a slightly lower temperature. With four sets of measurements repeated for the same preceding freeze rates, the $T_e - 20\,K$ result was (35 ± 20) mK ($k = 2$) lower than the $T_e - 2\,K$ result. The uncertainty of the comparison combined (a) the daily measurement repeatability for identical freezes (estimated standard deviation $\sigma_{n-1} = 5$ mK) with (b) the repeatability of the temperature difference between $T_e - 20\,K$ and $T_e - 2\,K$ ($\sigma_{n-1} = 9$ mK).

The effect of annealing a crucible at $T_e - 20\,K$ following freezing at $T_e - 20\,K$ showed no clear influence on melt quality or melt temperature up to 54 h anneal time. This could be due to the small number of measurements and the difficulty of detecting differences of only 20–30 mK.

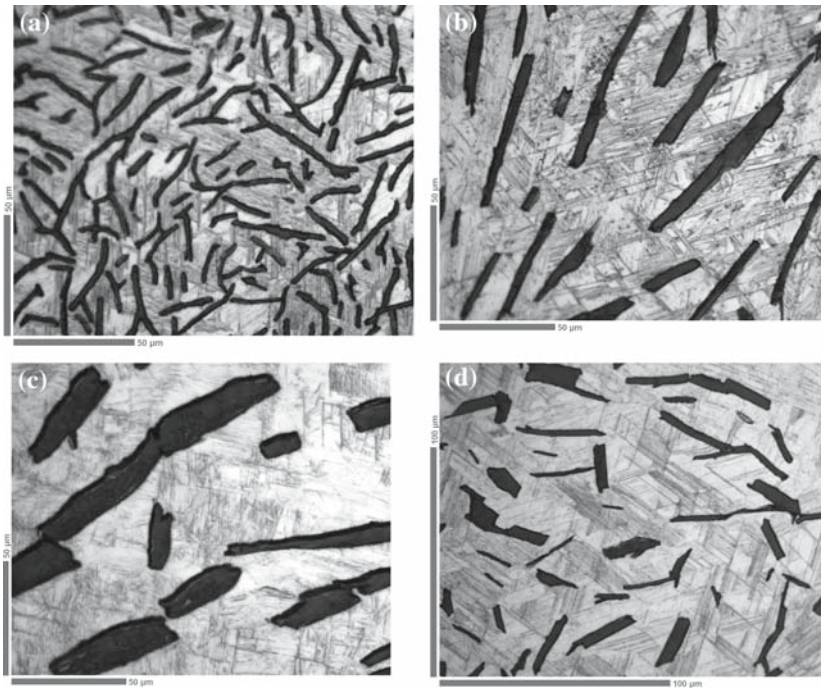

Fig. 2 Microstructure of polished and etched cobalt–carbon eutectic alloy frozen (annealed) at different rates: (**a**) frozen at $T_e - 20\,K$, (**b**) frozen at $T_e - 4\,K$, (**c**) frozen at $T_e - 2\,K$, and (**d**) frozen at $T_e - 20\,K$ and annealed for 54 h

The etched microstructure for samples solidified at different freeze rates is shown in Fig. 2a–c. Figure 2d shows a fast-frozen and annealed sample. The irregular appearance of the graphite phase arises from the directional nature of the graphite bonds, which give preferred directions of growth (faceting). The metallic bonds of the cobalt-rich matrix, in contrast, have little tendency to facet. There is a clear change in scale depending on the rate of solidification, which varied approximately from $0.25\,mm \cdot min^{-1}$ at the faster rate to $0.025\,mm \cdot min^{-1}$ at the slower. The annealed sample shows coarsening of the graphite flakes and increased separation. The scale of the microstructure appears most similar to the $T_e - 4\,K$ sample. The parallel lines in the matrix may be due to twinning.

Figure 3a, b shows the misorientation in samples frozen at $T_e - 2\,K$ and $T_e - 20\,K$. The orientation of a pixel is compared to the average of its neighbors. Any difference between pixels of more than 3° is assumed to be due to a grain or sub-grain boundary and is not included. The maps give an indication of the amount of residual strain left after solidification. The white areas correspond to missing data, either graphite or, in Fig. 3b, additional areas where the analysis software cannot determine the orientation. This may be due to rapid alternation of face-centered-cubic (fcc) and hexagonal-close-packed (hcp) atomic arrangements in the cobalt-rich phase (Fig. 5). Otherwise, the darker regions indicate more stress than the lighter areas. The fast-frozen sample shows much more strain within the matrix than the slow-frozen sample.

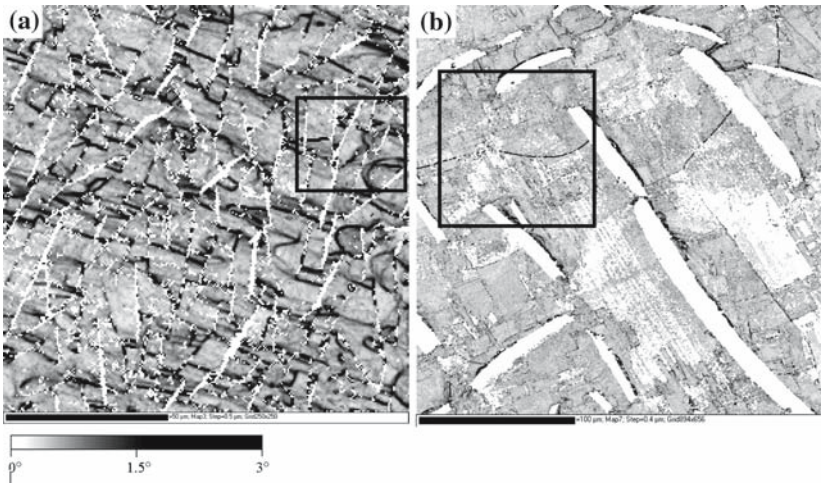

Fig. 3 Residual stress indicated by EBSD misalignment plots: (**a**) frozen at $T_e - 20\,K$ and (**b**) frozen at $T_e - 2\,K$

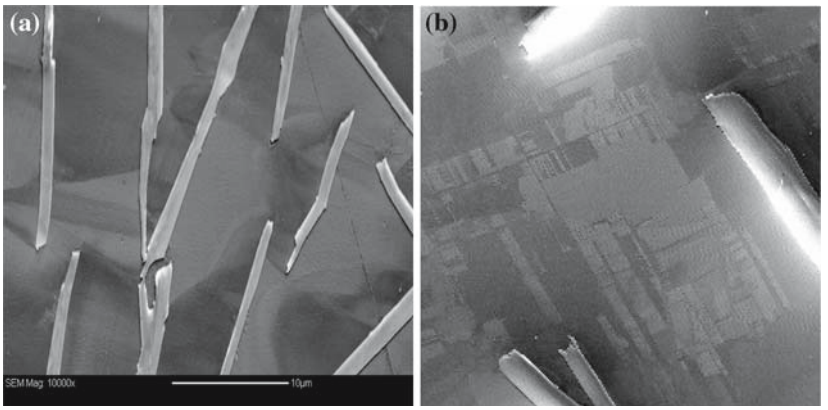

Fig. 4 Scanning electron microscope images of the samples: (**a**) fast freeze—area covered is shown in Fig. 3a and b slow freeze—area covered is shown in Fig. 3b

There is a flow pattern of graphite laths from top to bottom in Fig. 3a. The high stress areas form perpendicular to the laths. Figure 4a shows a higher magnification scanning electron microscope (SEM) image. The boundaries between the matrix areas of different contrast correspond to the highest residual strain in the misalignment plot. An SEM micrograph covering the same area as Fig. 3b shows a very regular microstructure. The EBSD scans indicate that this is due to alternating areas of fcc and hcp (Fig. 5).

4 Discussion

These results show that the melt curve of cobalt–carbon depends on the fixed-point thermal history. Two effects on the microstructure can be seen. First, the scale changes,

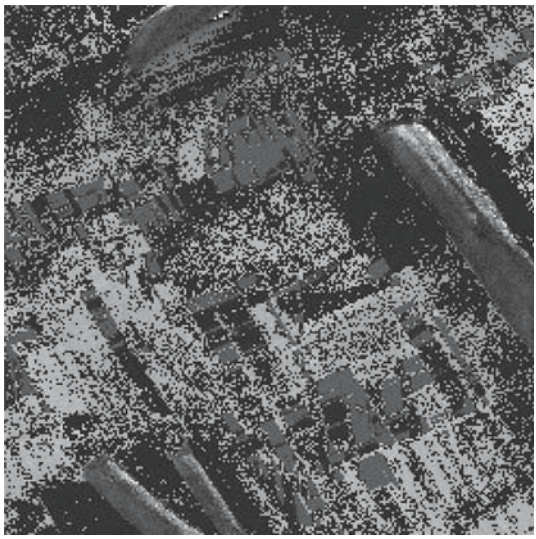

Fig. 5 EBSD image of Fig. 4b indicates a symmetric arrangement of fcc and hcp structures

with a decrease in the surface area of phase/grain boundaries for slower-frozen/annealed samples. Second, there is less damage/residual stress in the slower-frozen sample. The increased phase boundary area would be expected to result in a more pronounced rounding of the melt curve [7]. In [8], it was suggested that a grain size larger than 10–100 μm should be used to avoid pre-melting having an effect on melt temperature determination when using differential scanning calorimetry. This is about the scale of the microstructure reported here. The relative impact of the pre-melting effect should depend on the enthalpy of fusion, but—possibly apart from this aspect—it is not immediately apparent why the dependence on the preceding freeze is so different for different materials. There has to be a limit to the sub-grain growth, or the sample would segregate completely. This suggests that there is a lowest-energy configuration somewhere between fine and coarse microstructure. It may be that diffusion rates are fast enough at high temperatures so that all the freezes studied are close to the lowest energy state. It is also known that the inter-phase surface energy depends strongly on the degree of coherence between the lattices of the two phases, which will be material dependent.

The difference between melting temperatures following freezes carried out for set-points of $T_e - 2\,K$ and $T_e - 20\,K$ was about 35 mK. A contact thermometry cell in a well-insulated, enclosed furnace might use a $T_e - 2\,K$ freeze, while a radiation thermometry cell in an open furnace designed to work at much higher temperature might well use $T_e - 20\,K$, or even more. A difference of 35 mK between different uses is therefore quite possible, and is large enough change to warrant consideration for the highest accuracy needs. However, it is based on determining the melt from the POI. This is an arbitrary point that has been adopted as a matter of convenience. It is possible that the differences in melting temperature arise because an inappropriate feature of the melting curve is being used. The best temperature to use is the liquidus, i.e., the temperature as the last solid disappears. However, this is masked by the run-off

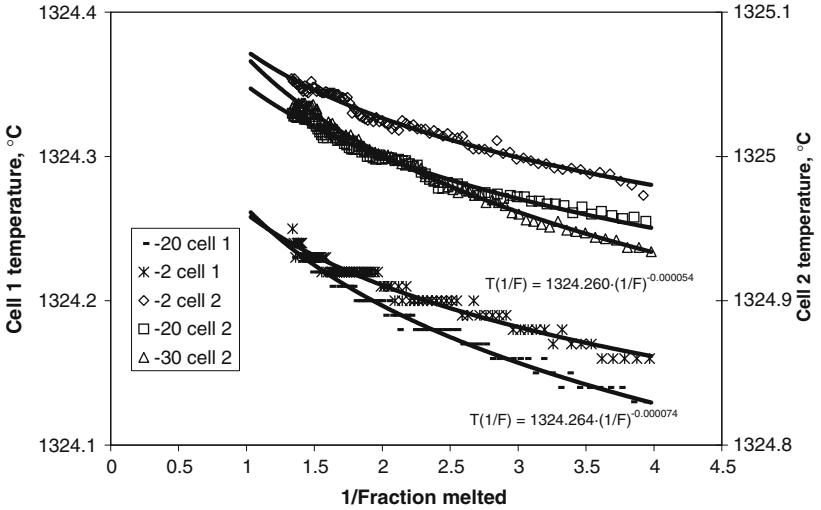

Fig. 6 Extrapolated $1/F$ plots for cobalt–carbon fixed-points frozen at different rates

at the end of melting [9,10]. To estimate the liquidus temperature, the following procedure is used: Once the start and end points of the melt have been identified, then the fraction melted (F) at any temperature can be found, assuming a constant rate of heat input. Following [11], the temperature is plotted against the inverse $1/F$, omitting the start and end data as being non-steady-state conditions. A function is fitted and then extrapolated to the liquidus ($1/F = 1$). According to [12], the thickness of a surface/interface disordered layer could diverge as ΔT^{-n}. The liquidus temperature T_{liq} can be determined by fitting a function $T(1/F) = T_{\mathrm{liq}}(1/F)^n$. A plot of such curves for the two cells is shown in Fig. 6 with extrapolated T_{liq} values for Cell 1. This method has the advantage that it has a more physical basis than the somewhat arbitrary POI value.

It has been assumed that segregation of impurities is not the cause of the variation in melting temperature. The finer microstructure increases the available channels for diffusion of impurities. It would be expected that fast freezing would reduce segregation and so the subsequent melting range, as is the case for conventional fixed points.

5 Conclusion

The importance of preceding freezing rate dependence for the best realization of cobalt–carbon fixed-points has been confirmed. There is a correlation between the microstructure and the melting behavior. As currently defined, there are differences in the measured melting temperature that are big enough to need consideration.

Acknowledgment The authors acknowledge the support of the Department of Trade and Industry, NMS Programme for Thermal Metrology (2004–2007).

References

1. Avavilable at http://www.bipm.fr/en/si/history-si/temp_scales/its-27.html. Accessed 3 October 2007
2. E. Woolliams, G. Machin, D. Lowe, R. Winkler, Metrologia **43**, R11 (2006)
3. Y. Yamada, B. Khlevnoy, Y. Wang, T. Wang, K. Anhalt, Metrologia **43**, S140 (2006)
4. W. Kurz, D.J. Fisher, *Fundamentals of Solidification*, 3rd edn. (Trans Tech Pubs., Aedermannsdorf, Switzerland, 1992), Chap. 5
5. N. Sasajima, Y. Yamada, P. Bloembergen, Y. Ono, in *Proc. TEMPMEKO 2004, 9th Int. Symp. on Temperature and Thermal Measurements in Industry and Science*, ed. by D. Zvizdic (FSB/LPM, Zagreb, Croatia, 2005), pp. 195–202
6. T. Wang, Y. Yamada, Y. Wang, P. Bloembergen, in *Proc. SICE Annual Conf.,* Okayama (2005), pp. 2739–2743
7. J. Frenken, P. Marée, J. van der Veen, Phys. Rev. B **34**, 7506 (1986)
8. V. Gusarov, Thermochim. Acta **256**, 467 (1995)
9. J. Anscin, Metrologia **38**, 1 (2001)
10. D. Lowe, Y. Yamada, Metrologia **43**, S135 (2006)
11. C. Plato, A. Glasgow, Anal. Chem. **41**, 330 (1969)
12. B. Pluis, D. Frenkel, J. van der Veen, J. Surf. Sci. **239**, 282 (1990)